ACS Pharmacology & Translational Science

pubs.acs.org/ptsci

Article

Comparison of the Tissue Distribution of a Long-Circulating Glucagon-like Peptide-1 Agonist Determined by Positron Emission Tomography and Quantitative Whole-Body Autoradiography

Published as part of the ACS Pharmacology & Translational Science virtual special issue "New Drug Modalities in Medicinal Chemistry, Pharmacology, and Translational Science".

Eduardo Felipe Alves Fernandes,*,‡ Jonas Wilbs,*,‡ Rene Raavé, Christian Borch Jacobsen, Hanne Toftelund, Hans Helleberg, Milou Boswinkel, Sandra Heskamp, Magnus Bernt Frederik Gustafsson, and Inga Bjørnsdottir

Cite This: *ACS Pharmacol. Transl. Sci.* 2022, 5, 616–624

Read Online

ACCESS | Metrics & More | Article Recommendations | Supporting Information

ABSTRACT: Positron emission tomography (PET) is a molecular imaging modality that enables non-invasive visualization of tracer distribution and pharmacology. Recently, peptides with long half-lives allowed once-a-week dosing of glucagon-like peptide-1 receptor (GLP-1R) agonists with therapeutic applications in diabetes and obesity. PET imaging for such long-lived peptides is hindered by the typically used short-lived radionuclides. Zirconium-89 (^{89}Zr) emerged as a promising PET radionuclide with a sufficiently long half-life to be applied for biodistribution studies of long-circulating biomolecules. A comparison between the biodistribution profiles obtained via ^{89}Zr-PET and the current standard, quantitative whole-body autoradiography (QWBA), will be valuable for the development of novel peptide drugs. We determined the PET biodistribution of a ^{89}Zr-labeled acylated peptide agonist of GLP-1R and compared it to the profile obtained by QWBA using analogous tritiated tracers for up to 1 week after administration. The plasma metabolic profile was obtained and identification was done for the tritiated tracers. We found that, at early time points, the biodistribution profiles agreed between PET and QWBA. At the latertime points, the ^{89}Zr tracer remained primarily trapped in the kidneys. The introduction of desferrioxamine (DFO) chelator reduced the peptide stability, and UPLC-MS analysis identified a circulating metabolite arising from DFO hydrolysis. Kidney accumulation of radiolabeled peptides and DFO metabolic instability may compromise biodistribution studies using ^{89}Zr-PET to support the development of new biopharmaceuticals. PET and QWBA biodistribution data correlated well during the absorption phase, but new and more stable ^{89}Zr chelators are needed for a more accurate description of the elimination phase.

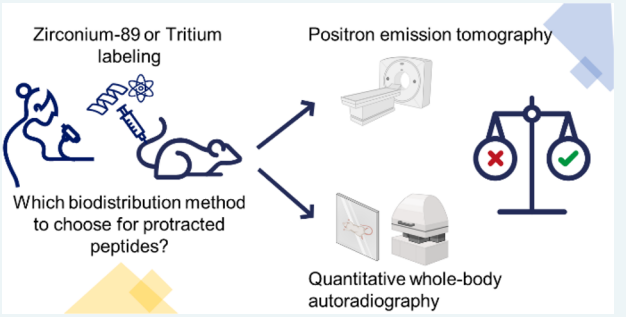

KEYWORDS: *positron emission tomography, quantitative whole-body autoradiography, peptides, biodistribution, zirconium-89*

Tissue distribution evaluation constitutes an essential part of the absorption, distribution, metabolism, and excretion (ADME) program of new drug candidates. Biodistribution studies guide development scientists and regulatory agencies about the extension of tissue exposure to the intended organs and potential safety concerns from off-targeting. As such, these studies could integrate both the efficacy and safety assessments of a new drug application and are conducted during the non-clinical or clinical development stages.[1]

Pharmaceutical companies and regulatory agencies consider quantitative whole-body autoradiography (QWBA) a preferred tissue distribution method for non-clinical studies of small molecules and biologics.[2,3] That is because QWBA images generate multi-organ quantitative tracer tissue distribution, at sub-millimeter resolutions, introducing minimal chemical modifications to the tested molecule.[3,4] In this method, a drug labeled typically with ^{3}H, ^{14}C, or ^{125}I is administered, and whole-body tissue slides are opposed to phosphor plates to capture and image the emitted photons. In practice, the procedure for obtaining QWBA images is labor-intensive and time-consuming, as each time point will require several tissue

Received: April 20, 2022
Published: June 30, 2022

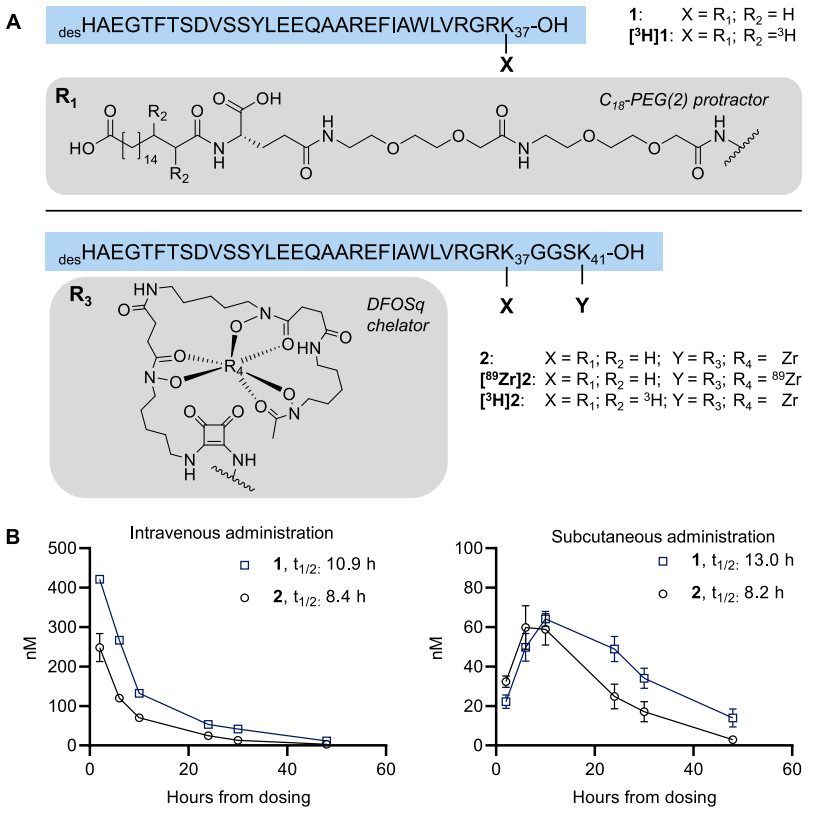

Figure 1. (A) Chemical structures of the peptides and radioactive tracers used in our study. Capital letters represent single-letter amino acid abbreviations, except for N, H, O, Zr, and C, representing atoms. $_{des}$H indicates the non-natural amino acid deamino-histidine and −OH the peptide carboxyl terminus. (B) Plasma pharmacokinetic curves of peptides **1**, and **2** after intravenous, and subcutaneous administration in rats at 20 nmol/kg dose. Data is shown as mean ± SD, n = 4 for **2**, and **1**, s.c.; n = 3 for **2**, i.v., and n = 1 for **1**, i.v.

slices and analyses. Therefore, non-invasive tissue distribution methods would be highly advantageous in drug development, in particular, for accessing early human data.

Positron emission tomography (PET) has been traditionally applied to cancer diagnostics, and recently it has also found applications in drug development, in particular for biomolecules.[5] When selecting a radionuclide for PET imaging, a critical parameter is the physical half-life of the radionuclide, which should ideally match the biological half-life of the labeled molecule.[6] With increased focus on long-circulating therapeutic modalities, such as antibodies and modified peptides, zirconium-89 (^{89}Zr) has emerged as a popular radionuclide due to its 3.3 days long physical half-life.[7] As a general principle, biodistribution data should derive from a tracer that closely resembles the parent molecule. In PET, ^{89}Zr labeling proceeds through the conjugation with a chelator moiety. Even for large molecules, such as monoclonal antibodies, the chelator position and chemistry can modify the drug properties; therefore, a more thorough evaluation is advocated.[8] The hydroxamate chelator desferrioxamine (DFO) has been typically used for ^{89}Zr complexation, from early applications of ^{89}Zr-PET to recent clinical trials.[9] Several studies, however, suggested that DFO instability after days of administration is a source of unspecific tracer uptake, in particular in the bones.[10,11] This has motivated the development of other chelator strategies, but so far only a few examples have been applied for tracers in clinical trials.[12,13]

Peptide modifications through lipidation have been a successful strategy to increase peptide stability and circulation times.[14] Semaglutide and liraglutide are potent glucagon-like peptide-1 receptor (GLP-1R) agonist peptides, which contain a fatty acid group that binds to serum albumin, leading to a protracted drug release and pharmacokinetics (PK).[15] In our previous work, we have developed and optimized the first ^{89}Zr PET tracer of a protracted GLP-1R receptor agonist peptide and demonstrated that it retains a high affinity to both GLP-1R and albumin and also similar *in vivo* pharmacodynamic properties after conjugation.[16]

Here, we use this model peptide to present the first tissue distribution comparison of a long-circulating peptide PET tracer with QWBA to validate PET as a non-invasive method in drug development. We investigate the influence of the chelator modification on PK, its metabolic stability, and how it shifted the tracer distribution 7 days after tracer administration via intravenous and subcutaneous routes.

RESULTS

Pharmacokinetic Characterization of Non-radioactive Peptides. Previously, the potent GLP-1R agonist peptide **1** (Figure 1) was modified to include a DFO chelator conjugated to a small C-terminal extension, generating peptide **2** after non-radioactive zirconium complexation.[16] To ensure that the tracer peptide remained stable in plasma for long-term PET imaging, we assessed possible PK differences and measured the concentration of **1** and **2** in rat plasma after subcutaneous (s.c.) and intravenous (i.v.) administration.

The half-life of **2** was indeed shorter than that of **1**, after both s.c. and i.v. administration (Figure 1B). Nevertheless, **2** retained the typically extended half-life of acylated peptides of approximately 10 h in rats, similar to semaglutide (7−12 h)

https://doi.org/10.1021/acsptsci.2c00075
ACS Pharmacol. Transl. Sci. 2022, 5, 616−624

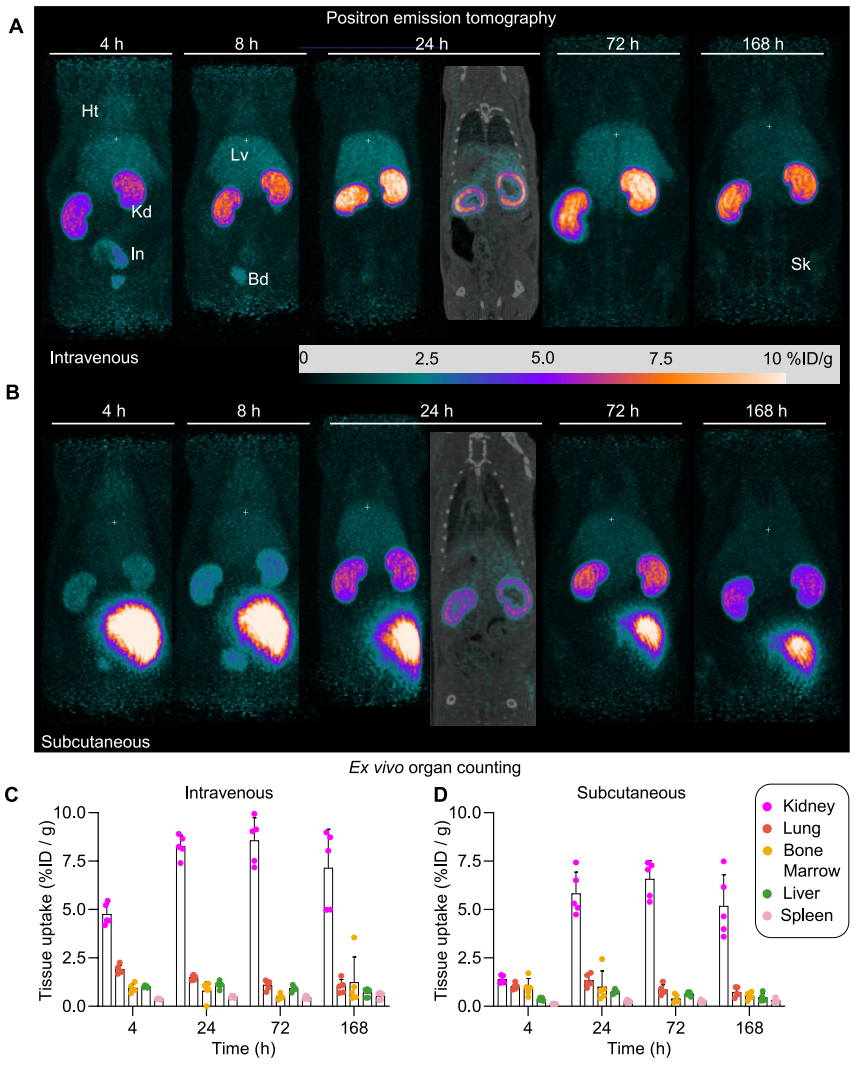

Figure 2. Positron emission tomography (PET) images of peptide [^{89}Zr]**2** after 4, 8. 24, 72, and 162 h of injection in rats. (A) Intravenous administration and (B) subcutaneous administration at doses of 17 MBq/kg (3 nmol/kg). Images are displayed as maximum intensity projections, coronal plane, representative of $n \geq 2$ per time point. Data is expressed as the percentage of the injected dose per gram (% ID/g). Abbreviations: ht, heart; kd, kidney; lv, liver; in, intestines; bd, bladder; sk, skeleton. (C, D) *Ex vivo* biodistribution in selected tissues after dosing with [^{89}Zr]**2** (3 nmol/kg) at 4, 24, 72, and 168 h after intravenous (C) or subcutaneous (D) injection. Data is expressed as the percentage of the injected dose per gram (% ID/g). Bar graphs data is shown as mean ± SD, n = 5, circles indicate the individual data points.

and much longer than unmodified GLP-1 (5 min) after i.v. administration.[15,17] Other pharmacokinetic parameters were also not substantially altered (Tables S1−S4). Hence, although we observed small PD and PK differences after modifying **1**, we considered that the 8.4 h elimination half-life of **2** is suitable for our long-term PET investigation.

One-Week Biodistribution Study of a ^{89}Zr-Labeled GLP-1R agonist Peptide by PET after Subcutaneous, and Intravenous Administration. PET images of [^{89}Zr]**2** after i.v. administration displayed high tracer uptake in the kidney cortex, lungs, urinary bladder, liver, and intestine after 4 h of injection (Figure 2A). Uptake in the heart was also observed, likely reflecting the albumin-binding tracer in blood. At 8 h, [^{89}Zr]**2** tissue distribution was similar to the 4 h time point, but with decreased signal from the intestines and increased signal from the kidney cortex. After 24 h, tracer concentration was maximum in the kidney cortex and predominated in the images after 72 and 168 h post injection. At 168 h, image-derived kidney uptake was approximately 7% injected dose per gram (ID/g). At the last two imaging time points, PET signal from the bones was observed (approximately 0.1% ID/g), which may indicate ^{89}Zr release.[10]

Tracer administration via s.c. route led to a comparable biodistribution pattern. Interestingly, PET images could clearly follow the slow tracer absorption from the subcutis depot. After 4 h, approximately 50% of the administered dose remained at the injection site; after 168 h, still, 10% of the initial dose was trapped in the subcutis (Figure 2B). *Ex vivo* tissue counting confirmed the PET imaging values, and both methods detected the same high uptake organs and similar kinetics (Figure 2C,D and Tables S5 and S6). For instance, the difference in kidney uptake between i.v. and s.c. dosed animals could be distinguished both in the *in vivo* PET image and after *ex vivo* counting. Evaluating the distribution of peptides **1** and **2** using tritiated analogs will help us to better determine what is the impact of the ^{89}Zr labeling in the distribution of **1**.

Quantitative Whole-Body Biodistribution of Tritiated Tracers after Subcutaneous and Intravenous Administration. Tritiated peptides [^{3}H]**1** and an analog of **2**, chelated to a non-radioactive zirconium isotope ([^{3}H]**2**), were

https://doi.org/10.1021/acsptsci.2c00075
ACS Pharmacol. Transl. Sci. 2022, 5, 616−624

produced for QWBA biodistribution assessment (Figure 1A). The fatty acid moiety is regarded as the most stable part of a protracted GLP-1 peptide; hence, the label in this position allows for the longest possible tracking of the parent compounds, and potential metabolites in circulation.[18] Distribution of [^{3}H]**2** was at maximum level 4 h after i.v. administration for most tissues. The highest tracer concentrations occurred in the blood, cerebrospinal fluid (CSF), and bile ducts and in highly perfused organs such as kidneys cortex, tooth pulp, and lungs (Figure 3A, Table S7). In the CSF and

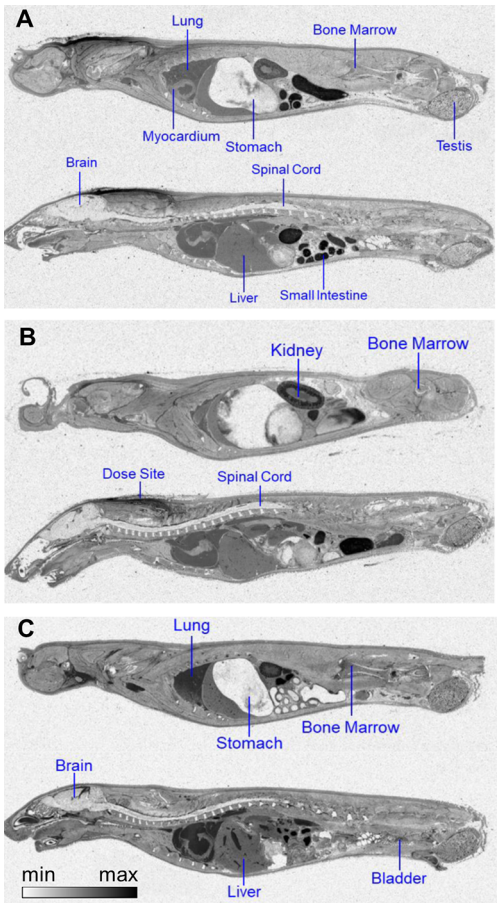

Figure 3. Quantitative whole-body autoradiography images of rats after administration of tritium-labeled tracers. (A) [^{3}H]**2**, 4 h after subcutaneous administration. (B) [^{3}H]**2**, 24 h after subcutaneous administration. (C) [^{3}H]**1**, 4 h after intravenous administration. Images display whole-body longitudinal sections distal (top) or proximal (bottom) to the animal midline. Dose: 30 nmol/kg (32 MBq/kg).

reproductive tissues, tracer concentration peaked at 8 h. CSF levels of both tracers were particularly high and even surpassed blood levels in the case of [^{3}H]**2**. After 24 h, [^{3}H]**2** was mainly distributed in the kidneys, and at 168 h, most of the tracer was cleared from the body. The distribution pattern of [^{3}H]**2** after s.c. administration resembled the i.v. However, the intensities of [^{3}H]**2** uptake after s.c. were, in general, lower than the i.v. at the first two time points and higher after 24 and 48 h after administration (Figure 3B, Table S8). After 72 h of s.c. administration, images displayed radioactivity predominately in the kidneys and at the dose site. After 1 week, kidneys uptake was below 0.1% ID/g, and radioactivity levels were below the quantification limit for all other tissues, except blood. The QWBA biodistribution of [^{3}H]**1** and [^{3}H]**2** after s.c. administration correlated well (Figure S1), and the highest tracer concentrations were observed in the same tissues (Tables S7−S9). [^{3}H]**2** concentrations were, in general, higher than [^{3}H]**1** in most tissues perhaps reflecting that **2** is more bioavailable than **1**.

Correlation between QWBA and PET Tracer Uptake. PET tracer uptake data of [^{89}Zr]**2** derived from gamma-counting of dissected organs to avoid errors arising from incorrect image segmentation and was compared to [^{3}H]**2** QWBA data for 10 major organs: blood, measured by liquid scintillation, liver, spleen, muscle, lung, bone marrow, skin, pancreas, and brain. We observed a good agreement between the organ distribution of the two tracers 4 h after administration, particularly after s.c. administration (Figure 4). Blood/plasma kinetics were also similar among the different tracers (Figure S2). Importantly, both methods indicated the kidneys, blood, and lungs as the organs with maximum tissue uptake. After 24 h, it is evident that kidney levels of [^{89}Zr]**2** are much higher than [^{3}H]**2**, and this difference increases until 72 h. Indeed, it is in the kidneys where the highest mismatch between PET and QWBA distribution occurs after both administration routes. For example, 72 h after i.v. dosing, kidney uptake was 1.0 and 8.6% ID/g for [^{3}H]**2** and [^{89}Zr]**2**, respectively. At the latest time point (168 h), [^{89}Zr]**2** uptake exceeds [^{3}H]**2** levels in all tissues. In a few instances, [^{3}H]**2** uptake is higher than that of [^{89}Zr]**2**, markedly in lung and blood, 4 h after i.v. dosing.

Metabolite Profiling and Identification. Plasma analysis revealed that the metabolism of [^{3}H]**1** and [^{3}H]**2** differed markedly. The HPLC profile of [^{3}H]**1** showed no intense circulating metabolites, except for [^{3}H]H_2O. In contrast, the metabolism of [^{3}H]**2**, originated several metabolites detected already at early time points. After s.c. administration, 80% of [^{3}H]**1** remained stable after 24 h, whereas [^{3}H]**2** rapidly degraded, and only 37% remained stable at this time point (Figure 5 and Figure S3). Both tracer peptides showed similar kinetics of [^{3}H]H_2O formation, consistent with a similar metabolism of the identical fatty acid side chains. In all cases, after 72 h [^{3}H]H_2O is the predominant source of radioactivity circulating in plasma.

Apart from [^{3}H]H_2O, [^{3}H]**2** metabolism generated at least three other radioactive components: [^{3}H]**2**-M(1−3) detected after both s.c. and i.v. administration. [^{3}H]**2**-M3 was the most abundant metabolite at 8 h post i.v. injection, accounting for 18% of the total peak area, and was more abundant in the s.c. samples (Figure 5). Mass spectrometry analysis of rat plasma, previously fractionated by HPLC, could not suggest any possible structures for [^{3}H]**2**-M1 and [^{3}H]**2**-M2. However, for the most intense metabolite; ([^{3}H]**2**-M3) a unique ion envelope with most abundant ion of m/z 1221.87 was observed, corresponding to a molecular weight of 4881.5 g/mol. We propose the structure of this metabolite as formed after an amide bond hydrolysis in the DFO chelator (spectra and structure in Figure 5D and Figures S5−S10). To control for any possible degradation from the sample processing, plasma from 24 h after s.c. administration was directly analyzed, without prior HPLC fractionation, and we found similar analytical data (Figures S8−S10), indicating that [^{3}H]**2**-M3 was formed in plasma.

https://doi.org/10.1021/acsptsci.2c00075
ACS Pharmacol. Transl. Sci. 2022, 5, 616−624

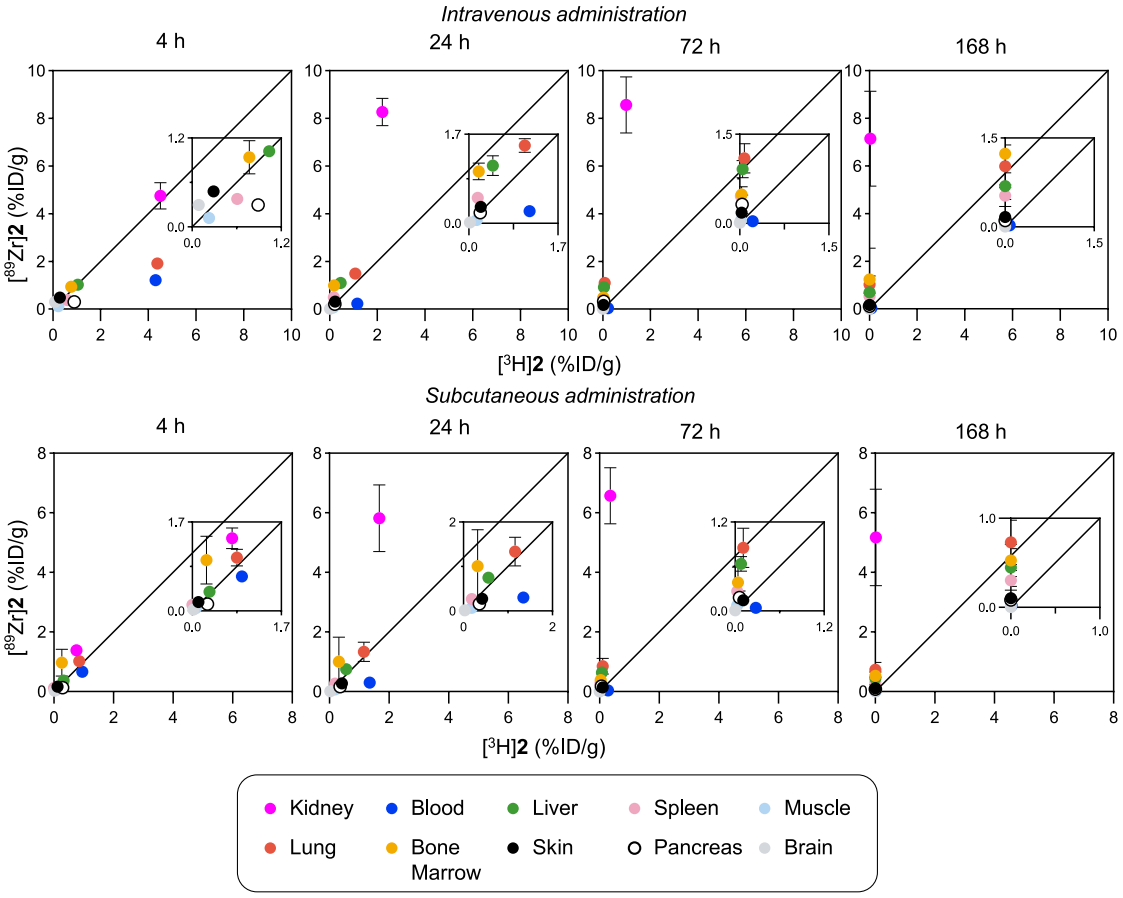

Figure 4. Correlation between tracer uptake in different organs using quantitative whole-body autoradiography (QWBA, tracer [^{3}H]**2**, 30 nmol/kg) or ex-vivo biodistribution after dosing with [^{89}Zr]**2** (3 nmol/kg) at 4, 24, 72, and 168 h after injection. The 45° line indicates the perfect correlation. Data is presented as mean ± SD, n = 1 for [^{3}H]**2** and $n \geq 3$ for [^{89}Zr]**2**.

DISCUSSION AND CONCLUSION

In our work, we envisioned that PET imaging with ^{89}Zr could estimate the biodistribution of long-lived GLP-1R agonists, as a translational methodology. ^{89}Zr labeling with a DFO squaramide has been shown to increase tracer stability and reduce bone accumulation and was defined as the labeling method of choice.[19,20] One requirement when developing tracer molecules for biodistribution imaging is minimal alteration of the parent molecule's properties, such as PK and receptor binding.[21] Although [^{89}Zr]**2** showed GLP-1R binding and *in vivo* pharmacology very similar to those of the parent compound **1** and the kinetics parameters of the two molecules were similar, a small but significant decrease in half-life was observed for [^{89}Zr]**2**. We attribute this difference to a potential reduction in albumin binding of the fatty acid side chain, induced by the DFO modification. Since the differences were minimal, we, therefore, concluded that modification of an albumin binding, long-circulating peptide, with Zr-DFO does not alter the PK and binding of the parent molecule to such extent that the tracer biodistribution would not be representative of the unmodified molecule.

PET imaging of [^{89}Zr]**2** provided the first evaluation of a ^{89}Zr-labeled, long-circulating peptide up to 7 days after s.c. and i.v. administration. At early time points, 4 and 24 h after dosing, [^{89}Zr]**2** distributed to lungs, which are known to express GLP-1R and clearance organs such liver and kidneys.[22] Signal in the pancreas, which expresses GLP1-R, was low, likely reflecting the low molar activity of [^{89}Zr]**2**. After 24 h, the PET signal localized mainly to the kidneys, a well-described process proposed to proceed via megalin-mediated renal re-absorption and subsequent entrapment in the lysosomes.[23] Interestingly, [^{89}Zr]**2** kidney uptake values are much lower than other GLP-1R radiometal ligands. For example, exendin-4 labeled with ^{89}Zr via a DFO chelator distributes to the kidney at values exceeding 150% ID/g, 24 h postinjection.[24] Such high values were also described for several chelators and isotopes combinations, indicating a general retention mechanism.[25] We attribute the comparatively low renal uptake of [^{89}Zr]**2** to its strong albumin binding, similarly to other protracted peptides.[26]

To evaluate PET as a tool to determine the biodistribution of investigational drugs, a comparison to the current standard technique QWBA is necessary. In general, PET and QWBA tissue uptake values agreed well at early time points, and both techniques pinpointed similar tissues containing low and high uptake levels. After 24 h the observed tissue uptake started to differ between the two techniques, particularly in the kidneys. The low kidney uptake of [^{3}H]**2** versus [^{89}Zr]**2** could indicate that the metabolite retained in the kidney originates from a cleavage after Lys 37 and contains the DFO chelator. Recently, the distribution pattern of different DFO degradation products was studied, and the complex [^{89}Zr]Zr(H_2O)DFO was found to accumulate in the kidneys, whereas other degradation products either were completely cleared or accumulated in bones.[27] Several potential challenges arise when comparing tracer distribution between QWBA and PET. QWBA outputs a

https://doi.org/10.1021/acsptsci.2c00075
ACS Pharmacol. Transl. Sci. 2022, 5, 616−624

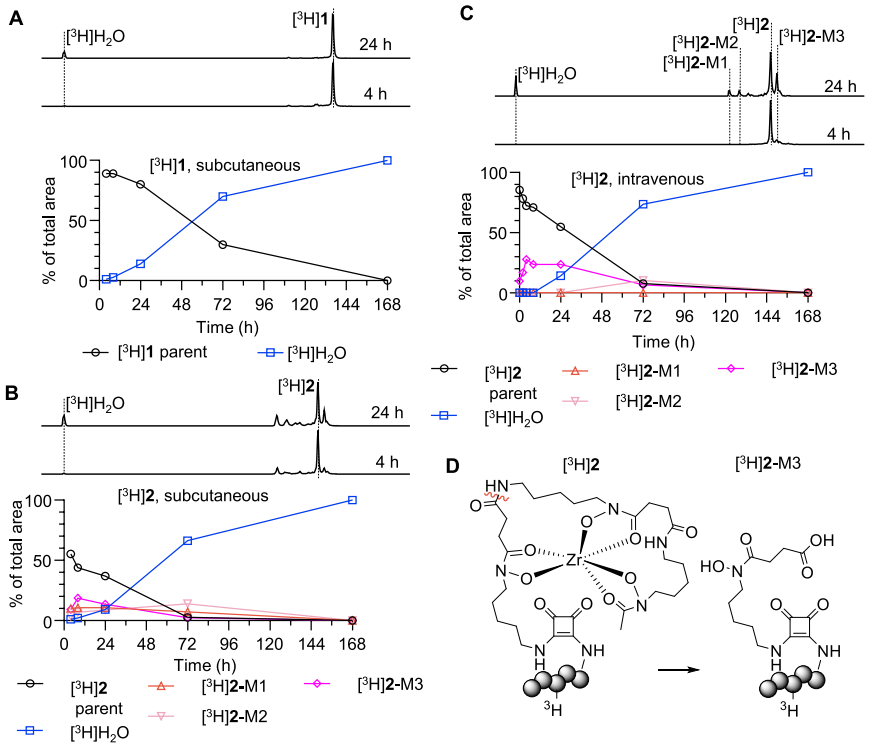

Figure 5. Metabolic profiling of peptides [^{3}H]**2** and [^{3}H]**1**. Fraction of parent [^{3}H]**1** (A) or [^{3}H]**2** (B, C) and metabolites remaining in rat plasma determined by radio-HPLC analysis. (D) Proposed chemical structure of the metabolite [^{3}H]**2**-M3 after mass spectrometry analysis. The proposed cleavage site is indicated in red.

bidimensional image where tissue uptake data is found in discrete organ regions. Tissue inhomogeneity may inflate or reduce the total organ uptake, as in the heart, where blood is present. In our study, we used *ex vivo* quantification of [^{89}Zr]**2** tissue uptake, and the image-derived data correlated with the *ex vivo* counting. Further evaluation, using co-registration with anatomical imaging (e.g., PET-CT or PET-MRI), may be necessary for full organ delineation and longitudinal study designs. Also, QWBA administered doses were 10-fold higher than PET, and it was required to obtain adequate sensitivity in the last time points. Apart from such challenges, the distribution of peptides [^{3}H]**2** and [^{89}Zr]**2** correlated well in several organs 24 h after administration.

Potential tracer degradation could bias the biodistribution conclusions and should be investigated. Typically, stability studies of ^{89}Zr PET tracers focus on demetalation using analytical methods such as radio-TLC without proposing the metabolite identities. In plasma, we found at least three different metabolites of [^{3}H]**2**, whereas no metabolite was detected for the parent peptide [^{3}H]**1**. The major metabolite [^{3}H]**2**-M3 was identified as a hydrolysis product of the DFO moiety, absent of zirconium, but with an intact peptide backbone and fatty acid side chain. Even though DFO instability is known and several alternatives and more stable chelators have been proposed, to our knowledge, this is the first time a DFO metabolite is assigned from *in vivo* samples using high-resolution mass spectrometry.[12,19] Notably, the structure we have identified ([^{3}H]**2**-M3) was recently proposed as a potential metabolite of DFO.[27] [^{3}H]**1** shares a similar amino acid backbone sequence and fatty-acid protractor to the approved GLP-1R agonist semaglutide. Gladly, the low number and abundance of plasma metabolites of [^{3}H]**1** correlated well with semaglutide data in rats, where metabolite exposures of 1−7% were observed.[18]

In conclusion, PET provides a promising technology for evaluating the biodistribution of long-circulating biologics. With optimal positioning of the chelator, properties such as PK and receptor binding are only slightly altered by the DFO modification. Physicochemical alterations from the parent compound are more likely to be expected when labeling short peptides. For early time points, up to 24 h PET gives nearly identical biodistribution results as the current standard technology QWBA. Moreover, PET enables a fast non-clinical to clinical translation, which provides a great aid in modern drug development focusing on human data. The main limitations of PET, as identified in this study, are *in vivo* stability or metabolism of the DFO chelator and kidney accumulation of the radiometal, which results in a skewed biodistribution at later time points. Therefore, novel and more stable ^{89}Zr chelators are still needed for the long-term assessment of biopharmaceuticals.

MATERIALS AND METHODS

Detailed descriptions of the materials and methods can be found in the Supporting Information.

Animals and Welfare. Animal studies were approved by the UK Animals Act of 1986 (License: PPL P61F851DB), the Radboud University local committee (Protocol 2017−0028) and the Danish animal welfare inspectorate (2014−15−0201−00388: C02). We used 69 Sprague−Dawley rats in total, weighing 200−300 g, and this studied complied with the ARRIVE guidelines.

Pharmacokinetic Analysis. Animals were dosed at 20 nmol/kg intravenously or subcutaneously. 200 μL blood samples were taken at 2, 6, 10, 24, 30, and 48 h processed

https://doi.org/10.1021/acsptsci.2c00075
ACS Pharmacol. Transl. Sci. 2022, 5, 616−624

to plasma, extracted and analyzed by UPLC-MS. Quantification was done using a calibration curve prepared from spiked plasma samples. Pharmacokinetic parameters were calculated using Phoenix WinNonlin version 8.1 (Certara L.P., USA), considering a non-compartmental model.

Tritium Quantitative Whole-Body Autoradiography. Peptides [^{3}H]**1**, and [^{3}H]**2** were dosed as a bolus i.v. or s.c. administration at 30 nmol/kg (32 MBq/kg). Animals were euthanized at 4, 8, 24, 72, and 168 h and frozen under isoflurane anesthesia (n = 1 per time point). Whole-animal longitudinal sections (30 μm) were taken onto Filmolux 610 tape and exposed to imaging plates (BAS TR2040, Fuji) for 14 days and visualized via radioluminography. Autoradiograms were analyzed and quantified by reference to calibration curves.

Metabolite Profiling and Identification. From animals dosed with tritium-labeled peptides, terminal blood samples were collected at 4, 8, 24, 72, and 168 h post dose, processed to plasma, extracted (recoveries >85%, Table S10), and analyzed by HPLC, coupled to a scintillation detector. For metabolic identification, extracted samples were analyzed by UPLC coupled to both a high-resolution mass spectrometer and a radioactivity detector.

Biodistribution of ^{89}Zr-Labeled Peptides and PET Imaging. Radiosynthesis of [^{89}Zr]**2** was done as previously described and formulated at 5 MBq/nmol.[16] Animals were administered i.v or s.c at doses of 17 MBq/kg (3 nmol/kg). For the *ex vivo* biodistribution, blood was sampled from the tail vein at 15 min, 30 min, 1, 2, 4, 6, 8, 24, 72, and 168 h after tracer administration. At 4, 24, 72, and 168 h after tracer administration selected tissues were collected and radioactivity was counted using a gamma counter (Wizard, PerkinElmer, USA). Values are expressed as the percentage of injected dose per gram tissue (% ID/g).

For PET, animals were imaged under general anesthesia (2−3% isoflurane/O_2) at 4, 8, 24, 72, and 168 h after injection using an Inveon small-animal PET scanner (Siemens Preclinical Solutions, Germany) using a 350−650 keV window (for 15 min at 4 and 8 h, for 20 min at 24 h, 30 min at 72 h, and 60 min at 168 h) followed by a 323 s transmission scan using a Co-57 source for attenuation correction. Reconstruction of scans was performed using Inveon Acquisition Workplace software with an iterative three-dimensional ordered subset expectation maximization using maximum a priori with shifted Poisson distribution algorithm with the following parameters: matrix, 256 × 256 × 161; pixel size, 0.4 × 0.4 × 0.8 mm with a corresponding beta of 0.05 mm. At the 24 h time point, animals were transferred for computer-tomography imaging (MiLabs μSPECT, The Netherlands). Images were exported to DICOM format, decay-correct to the time of injection and analyzed using the software Carimas (v. 2.10, Turku PET Center, Finland).

Data Analysis. Data analysis was performed using GraphPad Prism Version 9 and plotted as mean ± standard deviation for all the graphics.

■ ASSOCIATED CONTENT

Supporting Information

The Supporting Information is available free of charge at https://pubs.acs.org/doi/10.1021/acsptsci.2c00075.

Materials and methods details; Tables S1−S4, PK parameters of peptides **1** and **2**; Tables S5 and S6, *ex vivo* biodistribution of peptide [^{89}Zr]**2**; Tables S7−S9, tissue uptake of tritiated peptides from QWBA; Table S10, extraction coefficients for metabolic profiling analysis; Figure S1, correlation between tissue uptake of [^{3}H]**1** and [^{3}H]**2**; Figure S2, plasma kinetics of **1**, **2**, [^{3}H]**1**, [^{3}H]**2**, and [^{89}Zr]**2**; Figure S3, full chromatograms of metabolic profiling of [^{3}H]**1** and [^{3}H]**2**; Figures S4−S10, metabolic identification chromatograms and spectra; and Figure S11, chemical characterization of non-radioactive compounds (PDF)

■ AUTHOR INFORMATION

Corresponding Authors

Eduardo Felipe Alves Fernandes − *Global Drug Discovery, Novo Nordisk A/S, DK-2760 Måløv, Denmark;* orcid.org/0000-0003-3406-1357; Email: eduf@novonordisk.com

Jonas Wilbs − *Global Research Technologies, Novo Nordisk A/S, DK-2760 Måløv, Denmark*; Email: jwlb@novonordisk.com

Authors

Rene Raavé − *Radboudumc, Department of Medical Imaging − Nuclear Medicine, Radboud Institute for Molecular Life Sciences, 6500 HB Nijmegen, The Netherlands*

Christian Borch Jacobsen − *Isotope Chemistry, CMC Development, Novo Nordisk A/S, DK-2760 Måløv, Denmark;* orcid.org/0000-0002-7502-9831

Hanne Toftelund − *Global Drug Discovery, Novo Nordisk A/S, DK-2760 Måløv, Denmark*

Hans Helleberg − *Global Drug Discovery, Novo Nordisk A/S, DK-2760 Måløv, Denmark*

Milou Boswinkel − *Radboudumc, Department of Medical Imaging − Nuclear Medicine, Radboud Institute for Molecular Life Sciences, 6500 HB Nijmegen, The Netherlands*

Sandra Heskamp − *Radboudumc, Department of Medical Imaging − Nuclear Medicine, Radboud Institute for Molecular Life Sciences, 6500 HB Nijmegen, The Netherlands;* orcid.org/0000-0001-7250-0846

Magnus Bernt Frederik Gustafsson − *Global Research Technologies, Novo Nordisk A/S, DK-2760 Måløv, Denmark*

Inga Bjørnsdottir − *Global Drug Discovery, Novo Nordisk A/S, DK-2760 Måløv, Denmark*

Complete contact information is available at: https://pubs.acs.org/10.1021/acsptsci.2c00075

Author Contributions

‡E.F.A.F. and J.W. contributed equally to this work. E.F.A.F. designed the PET study, designed and performed the metabolic profiling and identification study, analyzed data from all experiments, and wrote the manuscript. J.W. designed the PK, QWBA, and PET studies, performed PK sample analysis, synthesized all non-radioactive molecules, and contributed to data analysis and writing of the manuscript. R.R., M.B., and S.H. designed and performed the PET study and data analysis. C.B.J. synthesized the tritium tracers for the QWBA study. H.T. designed and performed the *in vivo* part of the PK study. H.H. contributed to the metabolic identification study. M.B., F.G., and I.B. contributed to the design of all experiments, data analysis, and writing of the manuscript.

Notes

The authors declare no competing financial interest.

https://doi.org/10.1021/acsptsci.2c00075
ACS Pharmacol. Transl. Sci. 2022, 5, 616−624

■ ACKNOWLEDGMENTS

The research leading to these results received funding from the Innovative Medicines Initiatives 2 Joint Undertaking under grant agreement no. 116106. This Joint Undertaking receives support from the European Union's Horizon 2020 research and innovation program and EFPIA. The graphical abstract includes elements from biorender.com.

■ ABBREVIATIONS

ADME, absorption, distribution, metabolism, and excretion; DFO, desferrioxamine; GLP-1R, glucagon-like peptide-1 receptor; PET, positron emission tomography; PK, pharmacokinetic; QWBA, quantitative whole-body autoradiography; SD, standard deviation; SPECT, single-photon emission computed tomography; ^{89}Zr, zirconium-89

■ REFERENCES

(1) European Medicines Agency. ICH guideline M3(R2) on non-clinical safety studies for the conduct of human clinical trials and marketing authorization for pharmaceuticals, 2013. https://www.ema.europa.eu/en/ich-m3-r2-non-clinical-safety-studies-conduct-human-clinical-trials-pharmaceuticals (accessed January 2022).

(2) McEwen, A.; Henson, C. Quantitative whole-body autoradiography: past, present and future. *Bioanalysis* **2015**, *7* (5), 557−568.

(3) Solon, E. G. Use of radioactive compounds and autoradiography to determine drug tissue distribution. *Chem. Res. Toxicol.* **2012**, *25* (3), 543−555.

(4) Penner, N.; Xu, L.; Prakash, C. Radiolabeled absorption, distribution, metabolism, and excretion studies in drug development: why, when, and how? *Chem. Res. Toxicol.* **2012**, *25* (3), 513−531.

(5) Matthews, P. M.; Rabiner, E. A.; Passchier, J.; Gunn, R. N. Positron emission tomography molecular imaging for drug development. *Br. J. Clin. Pharmacol.* **2012**, *73* (2), 175−186. Gallamini, A.; Zwarthoed, C.; Borra, A. Positron Emission Tomography (PET) in Oncology. *Cancers (Basel)* **2014**, *6* (4), 1821−1889. Evans, J. D.; Jethwa, K. R.; Ost, P.; Williams, S.; Kwon, E. D.; Lowe, V. J.; Davis, B. J. Prostate cancer-specific PET radiotracers: A review on the clinical utility in recurrent disease. *Pract. Radiat. Oncol.* **2018**, *8* (1), 28−39.

(6) Wei, W.; Rosenkrans, Z. T.; Liu, J.; Huang, G.; Luo, Q.-Y.; Cai, W. ImmunoPET: Concept, Design, and Applications. *Chem. Rev.* **2020**, *120* (8), 3787−3851.

(7) Heskamp, S.; Raave, R.; Boerman, O.; Rijpkema, M.; Goncalves, V.; Denat, F. (89)Zr-Immuno-Positron Emission Tomography in Oncology: State-of-the-Art (89)Zr Radiochemistry. *Bioconjugate Chem.* **2017**, *28* (9), 2211−2223. La, M. T.; Tran, V. H.; Kim, H. K. Progress of Coordination and Utilization of Zirconium-89 for Positron Emission Tomography (PET) Studies. *Nucl. Med. Mol. Imaging* **2019**, *53* (2), 115−124.

(8) Ahn, S. H.; Vaughn, B. A.; Solis, W. A.; Lupher, M. L., Jr.; Hallam, T. J.; Boros, E. Site-Specific (89)Zr- and (111)In-Radiolabeling and In Vivo Evaluation of Glycan-free Antibodies by Azide-Alkyne Cycloaddition with a Non-natural Amino Acid. *Bioconjugate Chem.* **2020**, *31*, 1177.

(9) Meijs, W. E.; Herscheid, J. D. M.; Haisma, H. J.; Pinedo, H. M. Evaluation of desferal as a bifunctional chelating agent for labeling antibodies with Zr-89. *Int. J. Rad. Appl. Instrum. Part A, Applied Radiation and Isotopes* **1992**, *43* (12), 1443−1447. De Feo, M. S.; Pontico, M.; Frantellizzi, V.; Corica, F.; De Cristofaro, F.; De Vincentis, G. 89Zr-PET imaging in humans: a systematic review. *Clin. Transl. Imaging* **2022**, *10* (1), 23−36.

(10) Abou, D. S.; Ku, T.; Smith-Jones, P. M. In vivo biodistribution and accumulation of 89Zr in mice. *Nucl. Med. Biol.* **2011**, *38* (5), 675−681.

(11) Raavé, R.; Sandker, G.; Adumeau, P.; Jacobsen, C. B.; Mangin, F.; Meyer, M.; Moreau, M.; Bernhard, C.; Da Costa, L.; Dubois, A.; et al. Direct comparison of the in vitro and in vivo stability of DFO, DFO* and DFOcyclo* for 89Zr-immunoPET. *Eur. J. Nucl. Med. Mol. Imaging* **2019**, *46* (9), 1966−1977.

(12) Feiner, I. V. J.; Brandt, M.; Cowell, J.; Demuth, T.; Vugts, D.; Gasser, G.; Mindt, T. L. The Race for Hydroxamate-Based Zirconium-89 Chelators. *Cancers (Basel)* **2021**, *13* (17), 4466.

(13) Heskamp, S.; Raavé, R.; Boerman, O.; Rijpkema, M.; Goncalves, V.; Denat, F. 89Zr-Immuno-Positron Emission Tomography in Oncology: State-of-the-Art 89Zr Radiochemistry. *Bioconjugate Chem.* **2017**, *28* (9), 2211−2223.

(14) Muttenthaler, M.; King, G. F.; Adams, D. J.; Alewood, P. F. Trends in peptide drug discovery. *Nat. Rev. Drug Discovery* **2021**, *20* (4), 309−325.

(15) Knudsen, L. B.; Lau, J. The Discovery and Development of Liraglutide and Semaglutide. *Front. Endocrinol. (Lausanne)* **2019**, *10* (155), 155.

(16) Jacobsen, C. B.; Raavé, R.; Pedersen, M. Ø.; Adumeau, P.; Moreau, M.; Valverde, I. E.; Bjørnsdottir, I.; Kristensen, J. B.; Grove, M. F.; Raun, K.; et al. Synthesis and evaluation of zirconium-89 labelled and long-lived GLP-1 receptor agonists for PET imaging. *Nucl. Med. Biol.* **2020**, *82*−*83*, 49−56.

(17) Novo Nordisk. New Drug Application (209637) Pharmacology Review: Ozempic (semaglutide), 2017. https://www.accessdata.fda.gov/drugsatfda_docs/nda/2017/209637Orig1s000PharmR.pdf.

(18) Jensen, L.; Helleberg, H.; Roffel, A.; van Lier, J. J.; Bjørnsdottir, I.; Pedersen, P. J.; Rowe, E.; Derving Karsbøl, J.; Pedersen, M. L. Absorption, metabolism and excretion of the GLP-1 analogue semaglutide in humans and nonclinical species. *Eur. J. Pharm. Sci.* **2017**, *104*, 31−41.

(19) Chomet, M.; Schreurs, M.; Bolijn, M. J.; Verlaan, M.; Beaino, W.; Brown, K.; Poot, A. J.; Windhorst, A. D.; Gill, H.; Marik, J.; et al. Head-to-head comparison of DFO* and DFO chelators: selection of the best candidate for clinical 89Zr-immuno-PET. *Eur. J. Nucl. Med. Mol. Imaging* **2021**, *48* (3), 694−707.

(20) Rudd, S. E.; Roselt, P.; Cullinane, C.; Hicks, R. J.; Donnelly, P. S. A desferrioxamine B squaramide ester for the incorporation of zirconium-89 into antibodies. *Chem. Commun.* **2016**, *52* (80), 11889−11892.

(21) Boswell, C. A.; Tesar, D. B.; Mukhyala, K.; Theil, F.-P.; Fielder, P. J.; Khawli, L. A. Effects of Charge on Antibody Tissue Distribution and Pharmacokinetics. *Bioconjugate Chem.* **2010**, *21* (12), 2153−2163.

(22) Andersen, D. B; Grunddal, K. V; Pedersen, J.; Kuhre, R. E; Lund, M. L; Holst, J. J; Orskov, C. Using a Reporter Mouse to Map Known and Novel Sites of GLP-1 Receptor Expression in Peripheral Tissues of Male Mice. *Endocrinology* **2021**, *162*, 3.

(23) Velikyan, I.; Eriksson, O. Advances in GLP-1 receptor targeting radiolabeled agent development and prospective of theranostics. *Theranostics* **2020**, *10* (1), 437−461. Akizawa, H.; Uehara, T.; Arano, Y. Renal uptake and metabolism of radiopharmaceuticals derived from peptides and proteins. *Adv. Drug Delivery Rev.* **2008**, *60* (12), 1319−1328. Vegt, E.; Melis, M.; Eek, A.; de Visser, M.; Brom, M.; Oyen, W. J. G.; Gotthardt, M.; de Jong, M.; Boerman, O. C. Renal uptake of different radiolabelled peptides is mediated by megalin: SPECT and biodistribution studies in megalin-deficient mice. *Eur. J. Nucl. Med. Mol. Imaging* **2011**, *38* (4), 623−632.

(24) Bauman, A.; Valverde, I. E.; Fischer, C. A.; Vomstein, S.; Mindt, T. L. Development of 68Ga- and 89Zr-Labeled Exendin-4 as Potential Radiotracers for the Imaging of Insulinomas by PET. *J. Nucl. Med.* **2015**, *56* (10), 1569.

(25) Kaeppeli, S. A. M.; Schibli, R.; Mindt, T. L.; Behe, M. Comparison of desferrioxamine and NODAGA for the gallium-68 labeling of exendin-4. *EJNMMI Radiopharm. Chem.* **2019**, *4* (1), 9. Li, L.; Zhao, R.; Hong, H.; Li, G.; Zhang, Y.; Luo, Y.; Zha, Z.; Zhu, J.; Qiao, J.; Zhu, L.; et al. 68Ga-labelled-exendin-4: New GLP1R targeting agents for imaging pancreatic β-cell and insulinoma. *Nucl. Med. Biol.* **2021**, *102*−*103*, 87−96.

(26) Kaeppeli, S. A. M.; Jodal, A.; Gotthardt, M.; Schibli, R.; Béhé, M. Exendin-4 Derivatives with an Albumin-Binding Moiety Show Decreased Renal Retention and Improved GLP-1 Receptor Targeting.

Mol. Pharmaceutics **2019**, *16* (9), 3760−3769. Vegt, E.; Eek, A.; Oyen, W. J. G.; de Jong, M.; Gotthardt, M.; Boerman, O. C. Albumin-derived peptides efficiently reduce renal uptake of radiolabelled peptides. *Eur. J. Nucl. Med. Mol. Imaging* **2010**, *37* (2), 226−234.
(27) Guillou, A.; Earley, D. F.; Klingler, S.; Nisli, E.; Nüesch, L. J.; Fay, R.; Holland, J. P. The Influence of a Polyethylene Glycol Linker on the Metabolism and Pharmacokinetics of a 89Zr-Radiolabeled Antibody. *Bioconjugate Chem.* **2021**, *32* (7), 1263−1275.

■ NOTE ADDED AFTER ASAP PUBLICATION

In the version published ASAP on June 30, 2022, it could be interpreted that GLP1-R is extensively expressed in the liver, which has not been confirmed experimentally. There is controversy surrounding hepatic GLP-1R expression, with some studies reporting expression in hepatocytes, while others do not. The text in which this is discussed, in which ref 22 is cited, has been updated, along with the cited reference. In the updated ref 22, the liver showed a subtle reporter protein expression limited to the endothelial cells of sinusoids and central veins and intrahepatic branches of the portal vein. We Do not believe that this GLP-1R expression is sufficient to cause the observed PET signal in the liver in our study. The original ref 22 did not investigate GLP-1R expression in rodents, whereas the updated ref 22 does, and we believe this is more relevant for our discussion, as we performed our experiments in rodents. The updated version was published July 18, 2022.

https://doi.org/10.1021/acsptsci.2c00075
ACS Pharmacol. Transl. Sci. 2022, 5, 616−624